A small-molecule fragment that emulates binding of receptor and broadly neutralizing antibodies to influenza A hemagglutinin

Rameshwar U. Kadam[a] and Ian A. Wilson[a,b,1]

[a]Department of Integrative Structural and Computational Biology, The Scripps Research Institute, La Jolla, CA 92037; and [b]The Skaggs Institute for Chemical Biology, The Scripps Research Institute, La Jolla, CA 92037

Contributed by Ian A. Wilson, March 12, 2018 (sent for review February 5, 2018; reviewed by Jason McLellan and Robert M. Stroud)

The influenza virus hemagglutinin (HA) glycoprotein mediates receptor binding and membrane fusion during viral entry in host cells. Blocking these key steps in viral infection has applications for development of novel antiinfluenza therapeutics as well as vaccines. However, the lack of structural information on how small molecules can gain a foothold in the small, shallow receptor-binding site (RBS) has hindered drug design against this important target on the viral pathogen. Here, we report on the serendipitous crystallization-based discovery of a small-molecule *N*-cyclohexyltaurine, commonly known as the buffering agent CHES, that is able to bind to both group-1 and group-2 HAs of influenza A viruses. X-ray structural characterization of group-1 H5N1 A/Vietnam/1203/2004 (H5/Viet) and group-2 H3N2 A/Hong Kong/1/1968 (H3/HK68) HAs at 2.0-Å and 2.57-Å resolution, respectively, revealed that *N*-cyclohexyltaurine binds to the heart of the conserved HA RBS. *N*-cyclohexyltaurine mimics the binding mode of the natural receptor sialic acid and RBS-targeting bnAbs through formation of similar hydrogen bonds and CH-π interactions with the HA. In H3/HK68, *N*-cyclohexyltaurine also binds to a conserved pocket in the stem region, thereby exhibiting a dual-binding mode in group-2 HAs. These long-awaited structural insights into RBS recognition by a noncarbohydrate-based small molecule enhance our knowledge of how to target this important functional site and can serve as a template to guide the development of novel broad-spectrum small-molecule therapeutics against influenza virus.

influenza virus | drug design | X-ray crystallography | fragment | *N*-cyclohexyltaurine

Influenza viruses continue to be a major threat to the human population. Influenza epidemics are estimated to result in around 3–5 million cases of severe illness and about 290,000–650,000 deaths per annum and have resulted in over 50–100 million deaths during the pandemic years of this and the last century, thereby imposing a huge toll both on human health and the economy worldwide (who.int/mediacentre/factsheets/fs211). Influenza infection is initiated by binding of the virus hemagglutinin surface glycoprotein (HA) to sialic acid receptors on host epithelial cells in the respiratory tract followed by internalization and membrane fusion (1). Structurally, HA is a homotrimer (~220 kDa) with a large extracellular domain composed of the distal head (HA1) and proximal stem (HA2) regions (2). HA is the most abundant glycoprotein on influenza viruses, and its receptor-binding domain (RBD) in the head region is the target for many neutralizing antibodies elicited by natural infection and by vaccination. Unfortunately, the highly variable nature of the RBD generally leads to elicitation of antibodies that are mainly strain-specific. Furthermore, the constant antigenic drift and shift in influenza viruses can make it difficult to predict the appropriate strains for inclusion in the seasonal vaccine (3, 4); thus, the uncertainty in effectiveness of the seasonal influenza vaccine for any given year (cdc.gov/flu/professionals/vaccination/effectiveness-studies.htm) (5).

The antiviral medications approved worldwide against influenza are the M2 ion channel inhibitors (Amantadine and Rimantadine) that block proton-conducting activity and neuraminidase (NA) inhibitors (Oseltamivir and Zanamivir), which prevent release of nascent virions (6). However, both are showing a decline in efficacy due to the emergence of drug-resistant viruses (7, 8). HA has so far not been successfully targeted by any of the globally approved small-molecule drugs. However, within the hypervariable receptor-binding domain (RBD) of HA, the relatively conserved receptor-binding site (RBS) engages sialic acid receptors on host cells (9). Discovery or design of small-molecule therapeutics that can specifically target this small, shallow, receptor-binding pocket has been challenging but, if successful, could provide long-awaited leads against a new target site on influenza virus that would block viral entry and counteract the emerging resistance in the current drugs to other targets.

The high incidence of emergence of resistance against the available therapeutic options has prompted researchers to actively develop new modalities against influenza (10, 11). Derivatives of the existing drugs have been developed (6), such as NA inhibitors (peramivir and laninamivir), influenza polymerase inhibitors (favipiravir), agents targeting glycosylation of HA (cyanovirin-N and nitazoxanide), and fusion inhibitors (Arbidol analogs) (12). Efforts have also been focused on designing analogs of the natural receptor sialic acid-containing lipids (13) and polymers (14) including sialic acid-conjugated dendritic polymers (15), sialyloligosaccharides containing poly L-glutamic acid backbones (16), and sialyllactose-carrying polystyrene (17). Crystal structures of the receptor–analog-based inhibitors in complex with HA have demonstrated

Significance

Influenza is a contagious and sometimes lethal disease of the human respiratory tract. Current preventative measures include annual vaccination and a limited number of antiviral drugs. However, the effectiveness of the seasonal vaccine is unpredictable, and resistance has been developing to all approved drugs. Therefore, novel influenza therapeutics with new targets and mechanisms are essential to protect against future pandemics, epidemics, and seasonal flu. Here, we report on the serendipitous discovery of a noncarbohydrate-based small-molecule *N*-cyclohexyltaurine that binds to the receptor-binding site of influenza virus hemagglutinin. Our structural findings provide much needed insights on how to effectively and specifically target the hemagglutinin receptor-binding site with small-molecule ligands, a goal which has evaded researchers for many years.

Author contributions: R.U.K. and I.A.W. designed research; R.U.K. performed research; R.U.K. and I.A.W. analyzed data; and R.U.K. and I.A.W. wrote the paper.

Reviewers: J.M., University of Texas at Austin; and R.M.S., University of California, San Francisco.

The authors declare no conflict of interest.

Data deposition: The atomic coordinates and structure factors have been deposited in the Protein Data Bank, www.pdb.org (PDB ID codes 6CF5 and 6CEX).

[1]To whom correspondence should be addressed. Email: wilson@scripps.edu.

This article contains supporting information online at www.pnas.org/lookup/suppl/doi:10.1073/pnas.1801999115/-/DCSupplemental.

Published online April 2, 2018.

that, although the sialic acid moiety bound similarly in the RBS for all the ligands, the rest of the added substituents interact with the hypervariable residues on the periphery of the site (18), which likely accounts for their strain specificity and propensity to develop resistance. Together these data suggest that a truly broad-spectrum small-molecule drug would have to specifically target only conserved residues within the RBS. Since mimicking sialic acid by carbohydrate-based analogs has not been successful in developing potent, broad-spectrum inhibitors, due to the very weak binding of the sialic acid receptor itself ($K_d \sim 3$–5 mM), it is important to explore noncarbohydrate-based small-molecule ligand space. However, the lack of structural information on noncarbohydrate small-molecule inhibitors of the HA RBS has hindered RBS-targeted drug design against this viral pathogen.

Here, we illustrate how a noncarbohydrate small molecule specifically interacts with the RBS without contacting the surrounding hypervariable residues. Crystal structures of group-1 (H5/Viet) and group-2 (H3/HK68) HAs in complex with *N*-cyclohexyltaurine show that this ligand mimics the binding mode and key interactions of sialic acid and RBS-targeting antibodies. *N*-cyclohexyltaurine also exhibits a dual-binding mode by also binding to a stem pocket specific to group-2 HAs. These structural data can be used to guide further development of *N*-cyclohexyltaurine–based analogs and inspire design of new noncarbohydrate inhibitors for treatment and prevention of influenza.

Results and Discussion

Crystal Structure of *N*-Cyclohexyltaurine in Complex with Group-1 H5/Viet HA. In the process of seeking to obtain higher-resolution X-ray data on avian-origin H5N1 A/Vietnam/1203/2004 (H5/Viet) HA, we found a condition that produced crystals that diffracted to 2.0-Å resolution (Table 1). During structure determination by molecular replacement, using H5/Viet HA bound to a stem-targeting antibody as a search model [Protein Data Bank (PDB) ID 4FQI)], we observed additional electron density in the HA RBS (Fig. 1 *A*

Table 1. Data collection and refinement statistics for *N*-cyclohexyltaurine complexes with H3 and H5 HAs

X-ray data	NCT-H3/HK68	NCT-H5/Viet
Data collection		
Beamline	APS-23-IDD	APS-23-IDD
Wavelength, Å	0.9796	1.0332
Space group	$C222_1$	$P2_1$
Unit cell, Å,°	a = 104.8, b = 151.6, c = 346.8	a = 72.6, b = 232.9, c = 72.6 β = 118.9
Resolution range, Å*	50–2.57 (2.61–2.57)	50–2.04 (2.08–2.04)
Observations	477,339	467,194
Unique reflections	87,259 (3,773)	131,851 (6,021)
Completeness, %	98.3 (86.8)	98.4 (88.9)
I/σ(I)	21.4 (5.4)	29.3 (6.9)
R_{sym}[†]	0.11 (0.27)	0.04 (0.16)
R_{pim}[‡]	0.04 (0.12)	0.02 (0.08)
$CC_{1/2}$[§]	0.97 (0.92)	0.99 (0.97)
Redundancy	5.5 (4.0)	3.5 (2.9)
Refinement		
Resolution, Å	47.74–2.57	37.58–2.04
No. reflections[¶]	87,157 (4,352)	131,782 (6,500)
R_{cryst}[#]/R_{free}[‖]	0.17/0.20	0.19/0.22
No. atoms		
Protein	11,675	11,998
Ligand/carbohydrate	104/419	38/126
Water/ions	746/30	1,331/0
Wilson B, $Å^2$	28	24
Average B value, $Å^2$		
Protein	31	30
Ligand	49 and 41**	45
Water/ions	32/57	36/-
RMSD from ideal geometry		
Bond length, Å	0.004	0.003
Bond angle, °	0.7	0.6
Ramachandran statistics, %[††]		
Favored	96.0	98.3
Outliers	0.2	0.0
PDB ID	6CEX	6CF5

*Parentheses refer to outer shell statistics.

[†]$R_{sym} = \Sigma_{hkl} \Sigma_i \mid I_{hkl,i} - \langle I_{hkl} \rangle \mid / \Sigma_{hkl} \Sigma_i I_{hkl,i}$, where $I_{hkl,i}$ is the scaled intensity of the *i*th measurement of reflection *h*, *k*, *l*, and $\langle I_{hkl} \rangle$ is the average intensity for that reflection.

[‡]$R_{pim} = \Sigma_{hkl} (1/(n-1))^{1/2} \Sigma_i \mid I_{hkl,i} - \langle I_{hkl} \rangle \mid / \Sigma_{hkl} \Sigma_i I_{hkl,i}$, where *n* is the redundancy.

[§]$CC_{1/2}$, Pearson correlation coefficient between two random-half datasets.

[¶]Values in parentheses refer to number of reflections in test set.

[#]$R_{cryst} = \Sigma_{hkl} \mid F_o - F_c \mid / \Sigma_{hkl} \mid F_o \mid \times 100$, where F_o and F_c are the observed and calculated structure factors.

[‖]R_{free} was calculated as for R_{cryst}, but on a test set of 5% of the data excluded from refinement.

**B-values for *N*-cyclohexyltaurine binding to head and stem regions of H3/HK68 HA, respectively.

[††]Calculated using MolProbity (36).

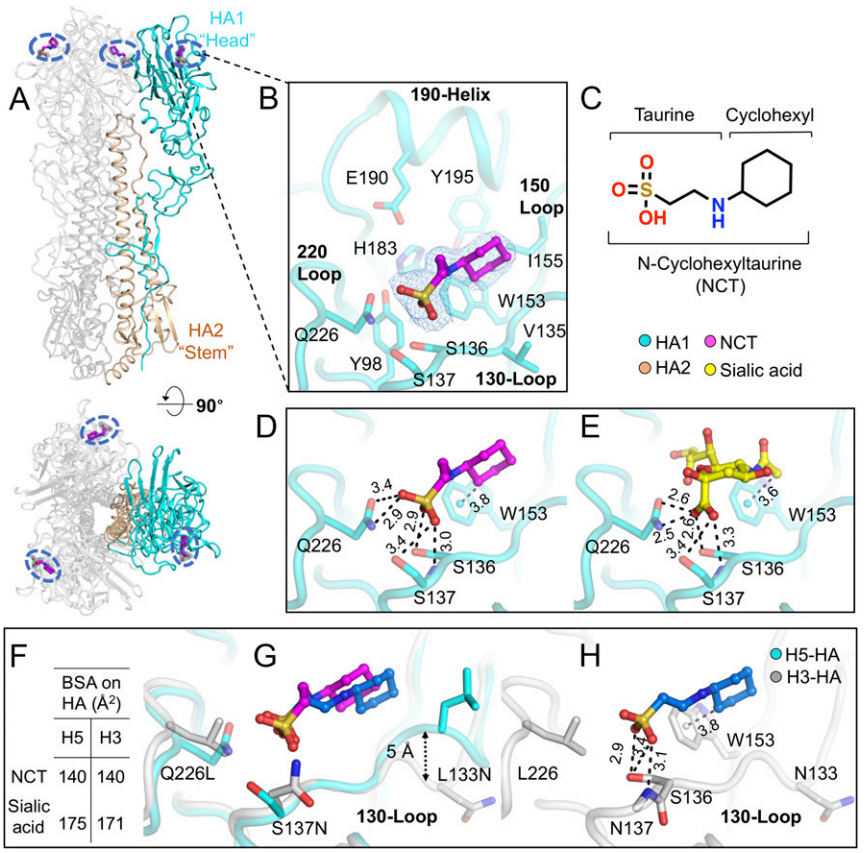

Fig. 1. Location of the *N*-cyclohexyltaurine binding site on influenza virus hemagglutinin. (*A*) Crystal structure of *N*-cyclohexyltaurine in complex with H5/Viet HA. HA trimer is represented as a cartoon with the one protomer (HA1, cyan and HA2, beige) and other two protomers in the transparent gray color. *N*-cyclohexyltaurine is shown in magenta sticks, and the receptor-binding sites (RBS) are highlighted using blue dotted circles. (*B*) Zoomed-in view of one of three binding sites with the 2Fo – Fc electron density map (blue mesh) contoured at 1σ around *N*-cyclohexyltaurine. (*C*) Molecular structure of *N*-cyclohexyltaurine. (*D* and *E*) Molecular interactions and receptor mimicry by *N*-cyclohexyltaurine in complex with H5/Viet HA. *N*-cyclohexyltaurine (magenta) recognizes the RBS and mimics the hydrogen bond and CH-π interactions made by sialic acid (yellow) with H5/Viet HA (cyan). (*F*) Buried surface area (BSA) of *N*-cyclohexyltaurine and sialic acid on H5 and H3 HAs. (*G* and *H*) Molecular interactions in the *N*-cyclohexyltaurine-H3/HK68 complex. (*G*) Superimposition of *N*-cyclohexyltaurine-bound structures with H5/Viet and H3/HK68 HAs. *N*-cyclohexyltaurine bound to H5 is in magenta sticks and bound to H3 in blue sticks. (*H*) Interaction of *N*-cyclohexyltaurine in the RBS of H3/HK68 HA. Hydrogen bond and CH-π interactions made by *N*-cyclohexyltaurine (blue sticks) with H3 RBS residues (gray cartoon) are represented in black dotted lines. The distances are measured in angstroms (Å).

and *B* and Fig. S1*A*). Analysis of the crystallization conditions revealed the presence of CHES buffer and PEG300. CHES buffer contains *N*-cyclohexyl-2-aminoethanesulfonic acid (CHES), also called *N*-cyclohexyltaurine, as the buffering agent. *N*-cyclohexyltaurine is a small-molecule fragment with molecular weight of 207.3 Daltons (pubchem.ncbi.nlm.nih.gov/compound/66,898) and is amphipathic, containing a hydrophilic charged moiety, taurine (2-aminoethanesulfonic acid), and a hydrophobic cyclohexyl group (Fig. 1*C*).

Refinement of the H5/Viet HA structure indicated a perfect fit for *N*-cyclohexyltaurine in the additional electron density present in the RBS (Fig. 1*B* and Fig. S2*A*). Although the RBD is hypervariable, the RBS contains several amino acids that are conserved over many influenza strains and subtypes (9). In H5 HA, the RBS comprises the central, highly conserved residues at its base (Y98, W153, H183) and surrounding residues in the 130-loop (V135, S136, S137), 150-loop (I155), 220-loop (Q226), and 190-helix (E190 to Y195) (Fig. 1*B*). The local architecture of the site is stabilized by a network of intramolecular hydrogen bonds formed between Y98, W153, Y195, and H183 that maintain the fixed geometry of this site despite the proximity of highly variable peripheral residues (9).

N-cyclohexyltaurine makes polar and nonpolar interactions with the highly conserved residues that frame the RBS (Fig. 1 *B* and *D*). Polar interactions include hydrogen bonds formed by the sulfonic acid of the taurine moiety with the sidechain and backbone atoms of S136, S137 from the 130-loop, Q226 from the 220-loop, and water-mediated H-bond interactions with the sidechain hydroxyl of Y98 from the floor of the pocket and Q226 from 220-loop (Fig. 1*D* and Figs. S3 and S4). The secondary amine functionality of *N*-cyclohexyltaurine also engages in water-mediated H-bonds with the carboxyl oxygen of E190 from the 190-helix (Fig. S4). The cyclohexyl group makes nonpolar interactions with the hydrophobic W153, I155, and L194 and CH-π interactions with the indole ring of W153 (Fig. 1 *B* and *D*). Such CH-π interactions can contribute ∼1 kcal/mol to the binding energy (19).

Receptor Mimicry by *N*-Cyclohexyltaurine in the RBS of Influenza HA. *N*-cyclohexyltaurine shows high structural mimicry of the influenza virus natural receptor, i.e., sialic acid, when interacting with the RBS of HA. The carboxylate group of sialic acid makes polar interactions with S136, S137 from the 130-loop and Q226 from the 220-loop, whereas the acetamido group interacts with W153 via CH-π interactions. The sulfonic acid and cyclohexyl groups of *N*-cyclohexyltaurine completely overlap with the carboxylate and acetamido groups of sialic acid, respectively, and make similar interactions with the conserved residues in the RBS (Fig. 1 *D* and *E* and Fig. S5). However, *N*-cyclohexyltaurine does not directly mimic the direct H-bond interactions of the glycerol sidechain of sialic acid with Y98, E190, and Q226 (9); but these interactions are mimicked via water-mediated H-bonds (Fig. S4). Overall *N*-cyclohexyltaurine buries about 140 Å^2 surface area on H5/Viet HA, which is comparable to sialic acid (175 Å^2) (Fig. 1*F*).

Structure-Based Validation of the *N*-Cyclohexyltaurine Binding Site on HA. To verify that the obtained *N*-cyclohexyltaurine-H5/Viet HA complex is not merely due to nonspecific binding of *N*-cyclohexyltaurine in the RBS of group-1 H5/Viet HA, we performed crystal-soaking experiments using HA from the 1968 pandemic strain of group-2 influenza A virus H3N2 A/Hong Kong/1/1968 (H3/HK68). Apo crystals obtained from a previously reported crystallization condition (20) were soaked for about 30 min at room temperature with *N*-cyclohexyltaurine at a final concentration of 20 mM (which is five times less than the original concentration of *N*-cyclohexyltaurine used in H5/Viet HA crystallization). The soaked crystals diffracted to 2.57-Å resolution (Table 1). Data processing and molecular replacement, with the apo structure of H3/HK68 HA as the search model (PDB ID 4FNK), clearly demonstrated additional electron density consistent

with *N*-cyclohexyltaurine in the RBS (Figs. S1*B* and S2*B*). This observation corroborated the original assignment of *N*-cyclohexyltaurine in the RBS of H5/Viet HA.

N-cyclohexyltaurine shows a similar binding mode and molecular interactions with RBS residues in group-2 H3/HK68 HA to those observed in group-1 H5/Viet HA (Fig. 1 *G* and *H* and Fig. S3). Key differences in the binding sites of H5/Viet vs. H3/HK68 HAs involve different residues, S137N and Q226L, in the 130- and 220-loops, respectively, of the RBS (Fig. 1*G* and Fig. S6). Because of these mutations, the sidechain-mediated hydrogen bonds made by the sulfonic acid group of *N*-cyclohexyltaurine with H5/Viet are not observed with N137 and L226 of H3/HK68 HA. However, interaction of the sulfonic acid group with the backbone amide of residue 137 was retained in H3/HK68. Similarly, the sidechain-mediated H-bond of S136 with the sulfonic acid group in the *N*-cyclohexyltaurine is also present in H3/HK68 (Fig. 1*H* and Fig. S3). Further, the CH-π H-bonds are identical in *N*-cyclohexyltaurine complexes with H3 and H5 HAs (Fig. 1 *D* and *H*). *N*-cyclohexyltaurine in complex H3/HK68 HA shows a more extended conformation in RBS that may be due to 5-Å downward shift of 130-loop region in H3 compared to H5 HAs (Fig. 1*G*). Overall, the surface area buried by *N*-cyclohexyltaurine upon binding to H3/K68 and H5/Viet is about 140 Å^2 (Fig. 1*F*). These results suggest that *N*-cyclohexyltaurine specifically recognizes the RBS of both group-1 and -2 influenza HAs.

Dual-Binding Mode of *N*-Cyclohexyltaurine in Group-2 H3/HK68 HA. Analysis of *N*-cyclohexyltaurine-H3/HK68 HA structure revealed further additional electron density in a conserved hydrophobic pocket in the stem region of H3/HK68 HA (Fig. 2 and Figs. S1*C* and S2*C*). Previously, this pocket has been characterized as the binding site for small-molecule fusion inhibitors of HA, *tert*-butyl hydroquinone (TBHQ) (21) and Arbidol (22). This binding pocket is easily accessible in group-2 HAs, but the presence of group-specific conformational differences in this region make the binding site largely inaccessible in group-1 HAs (22). This binding site is located at the interface of two protomers within the HA trimer, with three identical binding sites per trimer. Consequently, *N*-cyclohexyltaurine binds with stoichiometry of three ligands per trimer (Fig. 2*A*). The binding site comprises residues from protomer 1 [HA1 *P293, F294*, and *K307*; HA2 R54-T59 (helix-A and loop-B); and W92-E103 (helix-C)] and protomer 2 [HA1 *I29′*, *K310′*, *Q311′* and HA2 residues D90′-A101’ (helix-C′)] [note, HA1 residues are indicated in italics throughout and HA2 in regular font; (′) refers to residues from protomer 2 of the HA trimer] (Fig. 2*B*). The apo conformation of this stem binding pocket in H3/HK68 HA does not pose any steric hindrance to *N*-cyclohexyltaurine. Therefore, no significant conformational changes or salt bridge alterations were observed in the *N*-cyclohexyltaurine–H3/HK68 complex, unlike the binding of Arbidol to group-2 HAs (22).

The interactions of *N*-cyclohexyltaurine with the stem pocket in the H3/HK68 HA can be grouped into two regions: the central hydrophobic pocket and polar-charged residues framing the top and bottom of the cavity. Due to the large number of surrounding nonpolar residues with the binding cavity, *N*-cyclohexyltaurine is positioned such that its cyclohexyl group occupies a cavity formed by the hydrophobic *I29′*, L55, L98′, L99, and A101’ (Fig. 2*B*), whereas the sulfonic acid moiety is partially exposed to solvent with its more exposed front-side surrounded by basic residues K58, *K307*, and *K310′* and the back-side with the hydrophobic *F294*, W92, and Y94’. Sulfonic acid and the secondary amine of *N*-cyclohexyltaurine make direct H-bond interactions with the sidechain amine of *K307* and backbone carbonyl of R54, respectively (Fig. 2*B* and Fig. S3). In two of the three binding sites on HA, *N*-cyclohexyltaurine shows alternate

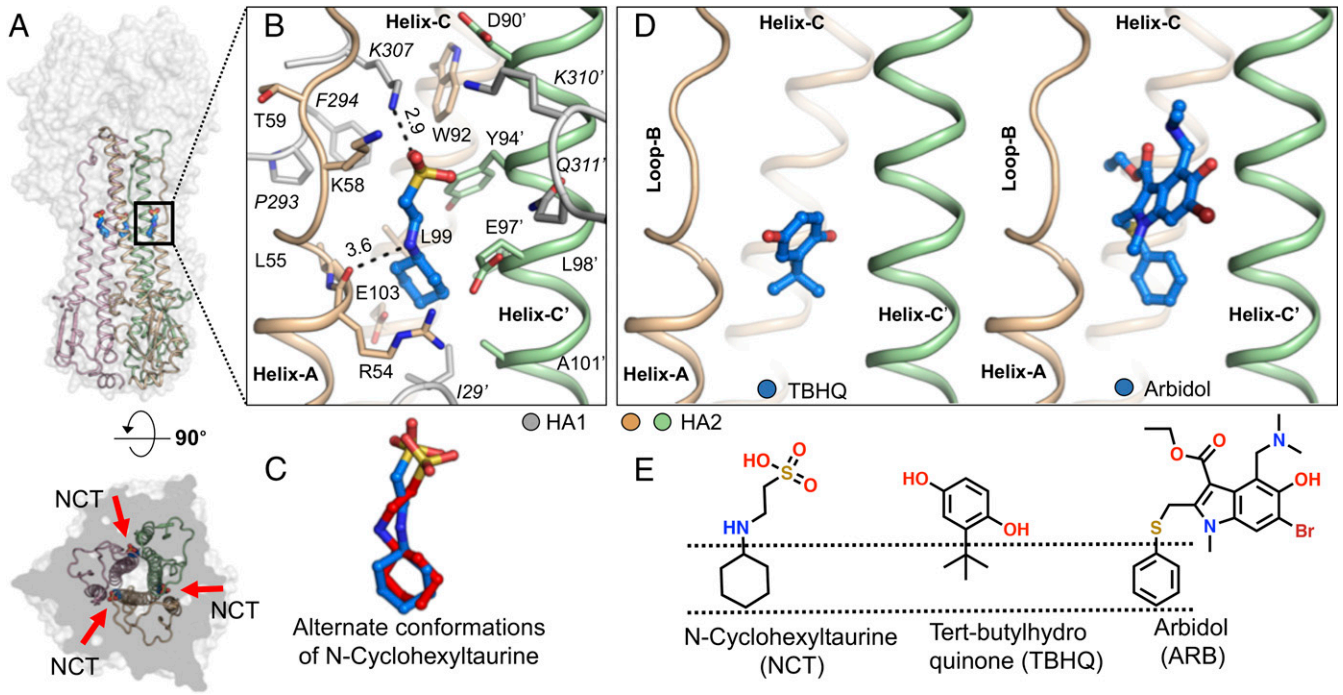

Fig. 2. Dual-binding mode of the *N*-cyclohexyltaurine in group-2 H3/HK68 HA. (*A*) Crystal structure of *N*-cyclohexyltaurine in complex with H3/HK68 HA. The HA trimer is represented as a transparent gray surface, whereas HA2 is represented in light pink, beige, and green colored secondary structure backbone traces in the different protomers, with *N*-cyclohexyltaurine in blue sticks. In the 90° rotation, three identical *N*-cyclohexyltaurine binding sites are shown as viewed along the threefold symmetric axis of HA trimer. (*B*) Zoomed-in view of one of the three binding sites of *N*-cyclohexyltaurine in H3/HK68 HA. The binding site consists of residues from HA1 (represented in the gray cartoon) and residues from HA2 helix-A and helix-C from protomer 1 (beige) and helix-C′ from protomer 2 (green). Hydrogen bond interactions are shown in black dotted lines and measured in Å. (*C*) Alternate conformations of *N*-cyclohexyltaurine (blue and red ball and sticks) in the binding site of H3/HK68 HA. (*D*) Crystal structure of H3 HA bound conformation of TBHQ (PDB ID 3EYK) and Arbidol (PDB ID 5T6N). (*E*) Molecular structures of *N*-cyclohexyltaurine, TBHQ, and Arbidol. The common hydrophobic moieties from all three ligands are highlighted within black dotted lines.

conformations, where the cyclohexyl moiety stays in position and the taurine moiety shows more flexibility in the binding sites (Fig. 2*C*). Analysis of the crystal structures of H3 HA bound conformation of known inhibitors TBHQ and Arbidol with the *N*-cyclohexyltaurine-H3/HA structure shows a consistent pattern of interactions with the HA stem pocket. Hydrophobic groups from all three ligands insert into the hydrophobic cavity, and the polar and charged groups are exposed toward the solvent (Fig. 2 *D* and *E*). Overall, *N*-cyclohexyltaurine buries ∼305 Å^2 of surface area in the stem pocket of H3/HK68 HA, whereas the buried surface areas for TBHQ are 235 Å^2, and those for Arbidol are 580 Å^2.

N-Cyclohexyltaurine Binding Mechanism Is Similar to the RBS-Targeting Antibodies. In addition to its high structural mimicry of sialic acid in the RBS, *N*-cyclohexyltaurine also shows striking similarity to the interaction and binding mode of broadly neutralizing antibodies targeting the HA RBS. Antibodies 5J8 (23), HC19 (24), CH65 (25), HC63 (26), and F045-092 (27) insert a carboxylate group from an aspartic acid at the tip of one of their complementarity-determining-region (CDR) loops (either CDR H2 or CDR H3) into the RBS of HA to form a network of polar interactions with residues from the 130- and 220-loops. Similar to the aspartic acid of the antibodies, the sulfonic acid group of *N*-cyclohexyltaurine occupies the same region and interacts with the 130- and 220-loop residues (Fig. 3*A*). Whereas antibodies C05 (20), HC19 (24), 8M2, and 2G1 (28) use hydrophobic tryptophan (W), tyrosine (Y), or phenylalanine (F) in their CDRs to make hydrophobic and π-stacking interactions with W153 and L194 in the RBS, the cyclohexyl group of *N*-cyclohexyltaurine is also positioned such that it also makes similar interactions with these RBS residues (Figs. 1*B* and 3*B*). The characteristic features of mimicking the binding modes of both the natural receptor sialic acid and RBS-targeting antibodies, along with its amphipathic nature, make *N*-cyclohexyltaurine a suitable candidate for drug development against influenza.

Perspective on Development of N-Cyclohexyltaurine. Although *N*-cyclohexyltaurine shows only millimolar binding toward H3/HK68 and H5/Viet04 HAs (Fig. S7), the structural information on the *N*-cyclohexyltaurine binding sites in group-1 H5/Viet and group-2 H3/HK68 HAs can now be exploited by structure-guided design to develop optimized influenza therapeutics. Since *N*-cyclohexyltaurine occupies the RBS in both group-1 and -2 HAs in addition to a conserved pocket in the stem of group-2 H3/HK68 HA, this molecule can be optimized individually for the two different targets on the HA.

As the RBS mediates the first event in the viral entry, blocking this critical first step by targeting the RBS is a very appealing strategy. Furthermore, as the RBS is a highly conserved site that is present across all subtypes of influenza A (group 1 and 2) and influenza B HAs, targeting this site would allow development of a truly universal small-molecule therapeutic. To optimize binding with the RBS, *N*-cyclohexyltaurine could be modified to interact with the hotspot pockets and displace the conserved water molecule(s) in the binding site (Fig. 3*C* and Fig. S4). The sulfonic acid group in the taurine moiety can be derivatized or substituted with a long bulky sidechain to target the pocket formed between 130- and 220-loops (hotspot 1) (Fig. 3*C*). The taurine moiety can be further elaborated to interact with hotspots 2 and 3 by mimicking the glycerol sidechain of sialic acid and to gain binding entropy by replacing water-mediated interactions with Y98 and E190 (Fig. 3*C* and Fig. S4). Another potential modification is to replace the cyclohexyl group with bulkier aromatic substitutions such as phenyl or other heterocycles, which could lead to improved occupancy of the conserved hydrophobic cavity around W153 (hotspot 4) and introduction of π–π stacking interactions. Dendrimer-like polymers may also be designed using *N*-cyclohexyltaurine as a template to generate multivalent ligands targeting the HA RBS (29, 30).

In the group-2–specific pocket in the upper HA stem, *N*-cyclohexyltaurine is positioned such that its cyclohexyl group occupies a cavity formed by hydrophobic residues, and the sulfonic acid moiety is partially exposed to solvent. To optimize interactions with this pocket, the cyclohexyl group could be modified by addition of bulky substitutions to improve hydrophobic interactions. Addition of a polar or charged group at this bulky substitution could introduce additional interactions with the E103 carboxyl. The sulfonic acid group and secondary amine may be replaced by bulkier polar substituents that can make direct H-bonds by displacing water molecules around helix-A and helix-C′ residues and to fit the binding pocket (Fig. S8), thereby resulting in a relative gain in binding entropy. Overall, *N*-cyclohexyltaurine represents a very interesting scaffold amenable to optimization for drug design and development of broad-spectrum inhibitors of influenza virus.

Conclusions

Serendipitous discovery of *N*-cyclohexyltaurine bound to influenza group-1 and -2 HAs has provided structural insights into how novel small-molecule ligands can target the highly conserved HA receptor-binding pocket. Despite being a noncarbohydrate small molecule, *N*-cyclohexyltaurine mimics the binding mode and key interactions of the natural receptor sialic acid as well as

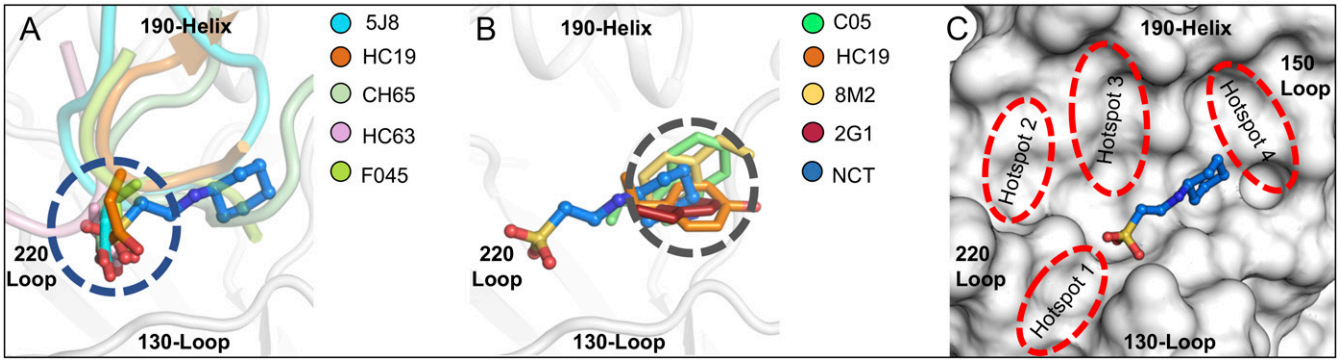

Fig. 3. Antibody mimicry by *N*-cyclohexyltaurine. (*A* and *B*) *N*-cyclohexyltaurine mimics the key interactions of RBS-targeting antibodies (note, the overall location of the binding site is depicted in Fig. 1). (*A*) The sulphonic acid group of *N*-cyclohexyltaurine (blue sticks) occupies the same region as that of RBS-targeting antibodies 5J8 (cyan, PDB ID 4M5Z), HC19 (orange, PDB ID 2VIR), CH65 (light green, PDB ID 3SM5), HC63 (light pink, PDB ID 1KEN), and F045 (lemon, PDB ID 4O58) that insert a carboxylate group from an Asp residue into the RBS (dashed blue circle). (*B*) The cyclohexyl group of *N*-cyclohexyltaurine (blue sticks) occupies the same region as that of antibodies, C05 (green, PDB ID 4FP8), HC19 (orange, PDB ID 2VIR), 8M2 (yellow, PDB ID 4HFU), and 2G1 (red, PDB ID 4HG4) that use hydrophobic residues (often aromatic) to target the RBS (dashed black circle). (*C*) Hotspot pockets around the *N*-cyclohexyltaurine-H3/HK68 complex. *N*-cyclohexyltaurine-bound conformation in RBS of H3/HK68 HA. *N*-cyclohexyltaurine is represented in blue, yellow, and red sticks, H3/HA in gray surface, and hotspots 1–4 are depicted as dotted red ellipses.

broadly neutralizing antibodies that target the RBS. In group-2 H3/HK68 HA, *N*-cyclohexyltaurine exhibits a dual-binding mode by additionally binding to a group–2–specific binding pocket in the HA stem that has previously been characterized as a binding site for the small-molecular fusion inhibitor Arbidol (22) and small-molecule fragment TBHQ (21). Thus, by delineating the binding mode of *N*-cyclohexyltaurine and its key interactions with HAs, the structures reported here can provide useful insights for optimizing this small-molecule fragment hit and guide development of broad-spectrum, noncarbohydrate-based, small-molecule therapeutics with mechanisms of action against influenza virus.

Materials and Methods

Expression and Purification of the Influenza Hemagglutinin. The hemagglutinin (HAs) used for crystallization study were expressed using baculovirus expression system as described previously (20). Briefly, each HA was fused with a gp67 signal peptide at the N terminus and to a BirA biotinylation site, thrombin cleavage site, foldon trimerization domain, and His_6-tag at the C terminus. Expressed HAs were purified using metal affinity chromatography using Ni- NTA resin. Further, the HAs were digested with trypsin (New England Biolabs, 5 mU trypsin per milligram HA, overnight at 4 °C) to produce uniformly cleaved HA1/HA2 and to remove the trimerization domain and His_6-tag. The digested material was purified by gel filtration using Superdex 200 16/90 column on an AKTA (GE Healthcare Life Sciences).

Crystallization and Structure Determination of *N*-Cyclohexyltaurine-H5/Viet and H3/HK68 HA Complexes. Gel filtration fractions containing H5/Viet and H3/HK68 HAs were concentrated to ∼5–10 mg/mL in 20 mM Tris, pH 8.0 and 150 mM NaCl. Crystallization screens were set up using the sitting drop vapor diffusion method with an HA concentration of ∼5 mg/mL for H5/Viet and ∼10 mg/mL for H3/HK68, either using our automated Rigaku CrystalMation robotic system at TSRI (for H5/Viet) or manually using a previously reported crystallization condition (for H3/HK68) (2.0 M ammonium sulfate, 100 mM sodium cacodylate, 200 mM sodium chloride, pH 6.5, 20 °C) (20). Within 3–7 d, diffraction-quality crystals were obtained. Crystallization of H5/Viet HA came from 100 mM of CHES (NCT), pH 9.5 and 40% vol/vol PEG600, 20 °C as precipitant. H3/HK68 crystals were soaked with a final concentration of ∼20 mM *N*-cyclohexyltaurine for about 30 min, cryoprotected with 5–15% glycerol, and then flash-cooled and stored in liquid nitrogen until data collection. The diffraction data were processed with HKL-2000 (31). Initial phases were determined by molecular replacement using Phaser (32) with HA models from H5/Viet (PDB ID 4FQI) and H3/HK68 (PDB ID 4FNK). Refinement was carried out in Phenix (33), alternating with manual rebuilding and adjustment in COOT (34). Detailed data collection and refinement statistics are summarized in Table 1.

Binding Affinity Measurements. Surface plasmon resonance (SPR) experiments were performed using a Biacore T200 instrument operating at 25 °C. Biotinylated HAs were covalently immobilized on streptavidin-coated, carboxymethylated dextran sensor surface (SA chip; GE Healthcare). Sialic acid and *N*-cyclohexyltaurine samples were prepared in the SPR running buffer (20 mM PBS, 137 mM NaCl, 0.05% P-20 surfactant, pH 7.4) (GE Healthcare). Binding constants were obtained from a series of injections of the ligands from concentration of 0.125 mM to 20 mM with a flow rate of 30 μL/min. Data from multicycle kinetics were analyzed using BIAevaluation software. The experimental sensorgrams were subtracted from background to yield curves representing specific binding. Binding affinities (K_D) were estimated from the concentration dependence of the observed steady-state responses and are reported in Fig. S7.

Structural Analyses. Two-dimensional depiction of the NCT binding sites on HAs were rendered using the Flatland Ligand Environment View (FLEV) mode of Lidia module in COOT (34). Surface areas buried on the HAs upon binding of *N*-cyclohexyltaurine and sialic acid were calculated with the Protein Interfaces, Surfaces and Assemblies (PISA) server at the European Bioinformatics Institute (35). Sialic acid bound to H5N1 (PDB ID 3ZP2) and H3N2 (PDB ID 1HGE) HAs were used for buried surface area calculations. MacPyMol (DeLano Scientific) was used to render structure figures. The final coordinates were validated using MolProbity (36).

ACKNOWLEDGMENTS. This work was supported by NIH Grants R56 AI117675 and R56 AI127371 (to I.A.W.). R.U.K. is grateful to the Swiss National Science Foundation for an Early Postdoc.Mobility fellowship. X-ray datasets were collected at the Advanced Photon Source, Argonne National Laboratory (beamline 23ID-D). The General Medicine and Cancer Institutes Collaborative Access Team (GM/CA CAT) is funded in whole or in part with federal funds from the National Cancer Institute (Y1-CO-1020) and National Institute of General Medical Sciences (NIGMS) (Y1-GM-1104). Use of the Advanced Photon Source was supported by the US Department of Energy, Basic Energy Sciences, Office of Science, under Contract DE-AC02-06CH11357. This is manuscript 29663 from The Scripps Research Institute.

1. Skehel JJ, Wiley DC (2000) Receptor binding and membrane fusion in virus entry: The influenza hemagglutinin. *Annu Rev Biochem* 69:531–569.
2. Wilson IA, Skehel JJ, Wiley DC (1981) Structure of the haemagglutinin membrane glycoprotein of influenza virus at 3 Å resolution. *Nature* 289:366–373.
3. Houser K, Subbarao K (2015) Influenza vaccines: Challenges and solutions. *Cell Host Microbe* 17:295–300.
4. Hensley SE (2014) Challenges of selecting seasonal influenza vaccine strains for humans with diverse pre-exposure histories. *Curr Opin Virol* 8:85–89.
5. Flannery B, et al. (2017) Interim estimates of 2016-17 seasonal influenza vaccine effectiveness–United States, February 2017. *MMWR Morb Mortal Wkly Rep* 66:167–171.
6. Das K (2012) Antivirals targeting influenza A virus. *J Med Chem* 55:6263–6277.
7. Moscona A (2009) Global transmission of oseltamivir-resistant influenza. *N Engl J Med* 360:953–956.
8. Sheu TG, et al. (2011) Dual resistance to adamantanes and oseltamivir among seasonal influenza A(H1N1) viruses: 2008-2010. *J Infect Dis* 203:13–17.
9. Weis W, et al. (1988) Structure of the influenza virus haemagglutinin complexed with its receptor, sialic acid. *Nature* 333:426–431.
10. Kadam RU, et al. (2017) Potent peptidic fusion inhibitors of influenza virus. *Science* 358:496–502.
11. Strauch EM, et al. (2017) Computational design of trimeric influenza-neutralizing proteins targeting the hemagglutinin receptor binding site. *Nat Biotechnol* 35: 667–671.
12. Wright ZVF, Wu NC, Kadam RU, Wilson IA, Wolan DW (2017) Structure-based optimization and synthesis of antiviral drug Arbidol analogues with significantly improved affinity to influenza hemagglutinin. *Bioorg Med Chem Lett* 27:3744–3748.
13. Guo CT, et al. (2002) An O-glycoside of sialic acid derivative that inhibits both hemagglutinin and sialidase activities of influenza viruses. *Glycobiology* 12:183–190.
14. Matrosovich M, Klenk HD (2003) Natural and synthetic sialic acid-containing inhibitors of influenza virus receptor binding. *Rev Med Virol* 13:85–97.
15. Reuter JD, et al. (1999) Inhibition of viral adhesion and infection by sialic-acid-conjugated dendritic polymers. *Bioconjug Chem* 10:271–278.
16. Totani K, et al. (2003) Chemoenzymatic synthesis and application of glycopolymers containing multivalent sialyloligosaccharides with a poly(L-glutamic acid) backbone for inhibition of infection by influenza viruses. *Glycobiology* 13:315–326.
17. Tsuchida A, et al. (1998) Simple synthesis of sialyllactose-carrying polystyrene and its binding with influenza virus. *Glycoconj J* 15:1047–1054.
18. Watowich SJ, Skehel JJ, Wiley DC (1994) Crystal structures of influenza virus hemagglutinin in complex with high-affinity receptor analogs. *Structure* 2:719–731.
19. Kadam RU, et al. (2013) CH-π "T-shape" interaction with histidine explains binding of aromatic galactosides to *Pseudomonas aeruginosa* lectin LecA. *ACS Chem Biol* 8: 1925–1930.
20. Ekiert DC, et al. (2012) Cross-neutralization of influenza A viruses mediated by a single antibody loop. *Nature* 489:526–532.
21. Russell RJ, et al. (2008) Structure of influenza hemagglutinin in complex with an inhibitor of membrane fusion. *Proc Natl Acad Sci USA* 105:17736–17741.
22. Kadam RU, Wilson IA (2017) Structural basis of influenza virus fusion inhibition by the antiviral drug Arbidol. *Proc Natl Acad Sci USA* 114:206–214.
23. Hong M, et al. (2013) Antibody recognition of the pandemic H1N1 Influenza virus hemagglutinin receptor binding site. *J Virol* 87:12471–12480.
24. Fleury D, Wharton SA, Skehel JJ, Knossow M, Bizebard T (1998) Antigen distortion allows influenza virus to escape neutralization. *Nat Struct Biol* 5:119–123.
25. Whittle JR, et al. (2011) Broadly neutralizing human antibody that recognizes the receptor-binding pocket of influenza virus hemagglutinin. *Proc Natl Acad Sci USA* 108:14216–14221.
26. Barbey-Martin C, et al. (2002) An antibody that prevents the hemagglutinin low pH fusogenic transition. *Virology* 294:70–74.
27. Lee PS, et al. (2014) Receptor mimicry by antibody F045-092 facilitates universal binding to the H3 subtype of influenza virus. *Nat Commun* 5:3614–3622.
28. Xu R, et al. (2013) A recurring motif for antibody recognition of the receptor-binding site of influenza hemagglutinin. *Nat Struct Mol Biol* 20:363–370.
29. Kadam RU, et al. (2011) A glycopeptide dendrimer inhibitor of the galactose-specific lectin LecA and of *Pseudomonas aeruginosa* biofilms. *Angew Chem Int Ed Engl* 50: 10631–10635.
30. Waldmann M, et al. (2014) A nanomolar multivalent ligand as entry inhibitor of the hemagglutinin of avian influenza. *J Am Chem Soc* 136:783–788.
31. Otwinowski Z, Minor W (1997) Processing of X-ray diffraction data collected in oscillation mode. *Methods Enzymol* 276:307–326.
32. McCoy AJ, et al. (2007) Phaser crystallographic software. *J Appl Cryst* 40:658–674.
33. Adams PD, et al. (2002) PHENIX: Building new software for automated crystallographic structure determination. *Acta Crystallogr D Biol Crystallogr* 58:1948–1954.
34. Emsley P, Cowtan K (2004) Coot: Model-building tools for molecular graphics. *Acta Crystallogr D Biol Crystallogr* 60:2126–2132.
35. Krissinel E, Henrick K (2007) Inference of macromolecular assemblies from crystalline state. *J Mol Biol* 372:774–797.
36. Chen VB, et al. (2010) MolProbity: All-atom structure validation for macromolecular crystallography. *Acta Crystallogr D Biol Crystallogr* 66:12–21.